

ELEPHANT: Extragalactic alErt Pipeline for Hostless AstroNomical Transients

P. J. Pessi^{1*}, R. Durgesh², L. Nakazono³, E. E. Hayes⁴, R. A. P. Oliveira⁵, E. E. O. Ishida⁶,
A. Moitinho⁷, A. Krone-Martins⁸, B. Moews^{9,10}, R. S. de Souza¹¹, R. Beck¹²,
M. A. Kuhn¹¹, K. Nowak¹¹, and S. Vaughan¹³ (for the COIN collaboration)

¹ The Oskar Klein Centre, Department of Astronomy, Stockholm University, AlbaNova 106 91, Stockholm, Sweden

² Independent Researcher, Ingolstadt, Germany

³ Instituto de Astronomia, Geofísica e Ciências Atmosféricas da USP, 05508-900, São Paulo, Brazil

⁴ Institute of Astronomy and Kavli Institute for Cosmology, Madingley Road, Cambridge, CB3 0HA, UK

⁵ Astronomical Observatory, University of Warsaw, Al. Ujazdowskie 4, 00-478 Warszawa, Poland

⁶ Université Clermont Auvergne, CNRS/IN2P3, LPC, F-63000 Clermont-Ferrand, France

⁷ CENTRA, Universidade de Lisboa, FCUL, Campo Grande, Edif. C8, 1749-016 Lisboa, Portugal

⁸ Donald Bren School of Information and Computer Sciences, University of California, Irvine, CA 92697, USA

⁹ Business School, University of Edinburgh, 29 Buccleuch Pl, Edinburgh, EH8 9JS, UK

¹⁰ Centre for Statistics, University of Edinburgh, Peter Guthrie Tait Rd, Edinburgh, EH9 3FD, UK

¹¹ Centre for Astrophysics Research, University of Hertfordshire, College Lane, Hatfield, AL10 9AB, UK

¹² Independent Researcher, Budapest, Hungary

¹³ School of Mathematical and Physical Sciences, Macquarie University, NSW 2109, Australia

April 30, 2024

ABSTRACT

Context. Transient astronomical events that exhibit no discernible association with a host galaxy are commonly referred to as hostless. These rare phenomena are associated with extremely energetic events, and they can offer unique insights into the properties and evolution of stars and galaxies. However, the sheer number of transients captured by contemporary high-cadence astronomical surveys renders the manual identification of all potential hostless transients impractical. Therefore, creating a systematic identification tool is crucial for studying these elusive events.

Aims. We present the Extragalactic alErt Pipeline for Hostless AstroNomical Transients (ELEPHANT), a framework for filtering hostless transients in astronomical data streams. It was designed to process alerts from the Zwicky Transient Facility (ZTF) as presented in the Fink broker; however, its underlying concept can be applied to other data sources.

Methods. We used Fink to access all the ZTF alerts produced between January/2022 and December/2023, selecting alerts associated with extragalactic transients reported in SIMBAD or TNS, as well as those classified as supernova (SN) or kilonova (KN) by the machine learning (ML) classifiers within the broker. We then processed the associated stamps using a sequence of image analysis techniques to retrieve hostless candidates.

Results. We find that $\lesssim 2\%$ of all analyzed transients are potentially hostless. Among them, only $\sim 10\%$ have a spectroscopic class reported on TNS, with Type Ia supernova being the most common class, followed by superluminous supernova. In particular, among the hostless candidates retrieved by our pipeline, there was SN 2018ibb, which has been proposed to be a Pair Instability SN candidate; and SN 2022ann, one of only five known SNe Icn. When no class is reported on TNS, the dominant classes are QSO and SN candidates, with the former obtained from SIMBAD and the latter inferred using the Fink ML classifier.

Conclusions. ELEPHANT represents an effective strategy to filter extragalactic events within large and complex astronomical alert streams. There are many applications for which this pipeline will be useful, ranging from transient selection for follow-up to studies of transient environments. The results presented here demonstrate the feasibility of developing specially crafted pipelines that enable a variety of scientific studies based on large-scale surveys. ELEPHANT is publicly available in the COINToolbox: https://github.com/COINtoolbox/extragalactic_hostless.

Key words. Methods: data analysis – Astronomical databases: miscellaneous – Stars: general – Methods: statistical

1. Introduction

Contemporary wide-field, untargated surveys that scan large portions of the sky on a regular basis, such as the All-Sky Automated Survey for Supernovae (ASAS-SN, Shappee et al. 2014), Gaia (Gaia Collaboration et al. 2016), the Asteroid Terrestrial-impact Last Alert System (ATLAS, Tonry et al. 2018) and the Zwicky Transient Facility (ZTF; Bellm et al. 2019), have sig-

nificantly increased the number of transients discovered nightly over the past decades¹. Such projects have not only increased the number of confirmed transients of known classes but have also facilitated the discovery of new classes of events (e.g., Druot et al. 2014; Kankare et al. 2017). Thus, the past decade has wit-

¹ See Yamaoka (2017) for numbers on the growth of discovered and classified supernovae from 1991 to 2015. For statistics on transient discovery and classification from 2016 onward, refer to <https://www.wis-tns.org/stats-maps>.

* e-mail: priscila.pessi@astro.su.se

nessed a significant increase and diversification of the transient sky landscape, populated by a myriad of objects (e.g. [Hambleton et al. 2023](#)).

Extragalactic transients can be described as the observational consequence of energetic events taking place outside the Milky Way. This description implies a progenitor population of astrophysical sources which should, in principle, be associated to a host galaxy. Nevertheless, a small fraction of transients seem to not be associated to any host and are thus considered *hostless* (e.g. [Qin et al. 2022, 2024](#)). In these cases, the host may remain undetected either because it is fainter than the survey’s limiting magnitude or because the transient was produced by a progenitor that achieved hypervelocity and escaped its host galaxy (e.g., [Martin 2006; Zinn et al. 2011](#)). Hostless transients have been associated with superluminous supernovae (SLSNe; e.g. [McCrum et al. 2015](#)), gamma-ray burst (GRBs; e.g. [Ho et al. 2020](#)), Fast X-ray transients (FXTs; e.g. [Gillanders et al. 2024](#)) and lensed transients (e.g. [Ryczanowski et al. 2020](#)), among others. Independently of the exact mechanism that rendered them hostless, such rare events represent an opportunity to further investigate peculiar astrophysical scenarios and may provide important clues regarding their local environment. They have already been used to discover low surface brightness galaxies (LSB, [Zinn et al. 2012](#)) and to study intra-cluster stellar populations ([Graham et al. 2015](#)).

Given such scientific potential, whenever a hostless transient is discovered, it sparks the interest of the astronomical community focused on rare events. In the past, the moderate number of discovered transients allowed thorough investigation of each candidate together with their associated hosts (e.g., [Filippenko 1997; Baldwin et al. 1981](#)). Nowadays, untargeted searches are discovering transients in fainter and more distant host galaxies, substantially increasing their numbers and rendering it impossible to study all of them in detail. As an example, ZTF currently detects a few hundred thousand transient candidates per night, while the upcoming Vera C. Rubin Observatory Legacy Survey of Space and Time (LSST) is expected to detect around 10 million per night over a period of 10 years ([Bellm et al. 2019](#)). In this context, it became necessary to develop automated frameworks for mining large astronomical datasets.

In this work, we introduce the Extragalactic aLErt Pipeline for Hostless Transients (ELEPHANT), whose goal is to enable automatic identification of confirmed or potential extragalactic events without an obvious host association. It significantly reduces the number of candidates requiring visual inspection, thus allowing an optimal allocation of expert time and follow-up resources. ELEPHANT employs a range of established image processing techniques to analyze image stamps associated with each transient, assessing the likelihood of a host’s presence. We detail the components of our pipeline and discuss a number of noteworthy candidates identified during its development. We visually inspected candidates with an associated spectroscopic classification available on the Transient Name Server (TNS²) to confirm their hostless nature. This process also helped us define statistical thresholds to apply to the rest of the sample. We found that less than $\lesssim 2\%$ of the analyzed sample is potentially hostless, with the most common classes of hostless candidates being QSOs, Type Ia SN, and SLSN. Some hostless candidates identified by our pipeline, which present interesting features, had already been thoroughly discussed in the literature (see Section 4). Our results illustrate the potential of the pipeline if applied to more recent data. We are currently working in integrating it to

the Fink broker ([Möller et al. 2021](#)), which will allow processing ZTF alert stream in real time and increase the chances of identifying hostless transients while they are still bright enough for spectroscopic follow-up.

This paper is organized as follows: Section 2 outlines the data selected for this analysis. Section 3 describes the ELEPHANT workflow. Results are presented in Section 4 and conclusions in Section 5.

2. Data

We use image data available within alerts distributed by ZTF. An alert package is produced when the difference imaging pipeline identifies a transient source. It includes photometric history, metadata, and three stamps: the original reference image – *template*, the new observation – *science*, and the difference image – *difference* ([Bellm et al. 2019; Masci et al. 2019](#)). This information is distributed nightly to community brokers, whose task is to filter, add value, and redistribute the alerts to domain experts. This work uses the alert stream information as provided by the Fink broker ([Möller et al. 2021](#)), however the pipeline is flexible enough to be used with other data sources³.

We retrieved all alerts processed by Fink between January/2022 and December/2023. The data set contained 70 176 557 alerts, which correspond to 17 683 691 objects. Approximately 50% of these have an associated classification. We only keep events associated with an extragalactic transient classification, including all classes of active galactic nuclei (AGN), supernovae (SNe), and kilonova candidates, among others (the complete list of the classes considered for this work can be found in our repository⁴). The classifications provided by Fink are obtained via cross-match with SIMBAD⁵ ([Wenger et al. 2000](#)), the Transient Name Server (TNS), or produced by machine learning (ML) algorithms used by the broker ([Möller & de Boissière 2020; Leoni et al. 2022; Biswas et al. 2023](#)). In case a cataloged classification is available, we consider it to be final. However, ML-based classifications are given per alert. Since one object can produce many alerts, this sometimes results in different classes associated with the same astrophysical source. When selecting sources for which only ML classification is available, the final class was chosen by majority vote, taking into account all alerts associated with the same object.

We exclude alerts with no associated classification or associated with galactic transients such as variable stars or objects present in the Minor Planet Center⁷. Since we are only interested in hostless events, we also considered cross-match with the MANGROVE catalog ([Ducoin et al. 2020](#)) and removed any object associated with a known host, even if the host galaxy association is tentative. We keep only $\sim 3.5\%$ of the original alerts by applying these conditions. To eliminate potentially bogus events, we only consider transients with two or more alerts, meaning that they will have more than one associated set of stamps. The stamps are typically 63×63 pixels with the detected transient located at the center. Smaller alerts are produced in rare cases, normally related to detector edge effects or due to defects in the

³ Other known community brokers include ALERCE ([Förster et al. 2021](#)), AMPEL ([Nordin et al. 2019](#)), ANTARES ([Matheson et al. 2021](#)), Babamul, LASAIR ([Williams et al. 2024](#)) and Pitt-Google.

⁴ https://github.com/COINtoolbox/extragalactic_hostless

⁵ <https://simbad.cds.unistra.fr/simbad/>

⁶ <https://www.wis-tns.org/>

⁷ <https://minorplanetcenter.net/about>

² <https://www.wis-tns.org/>

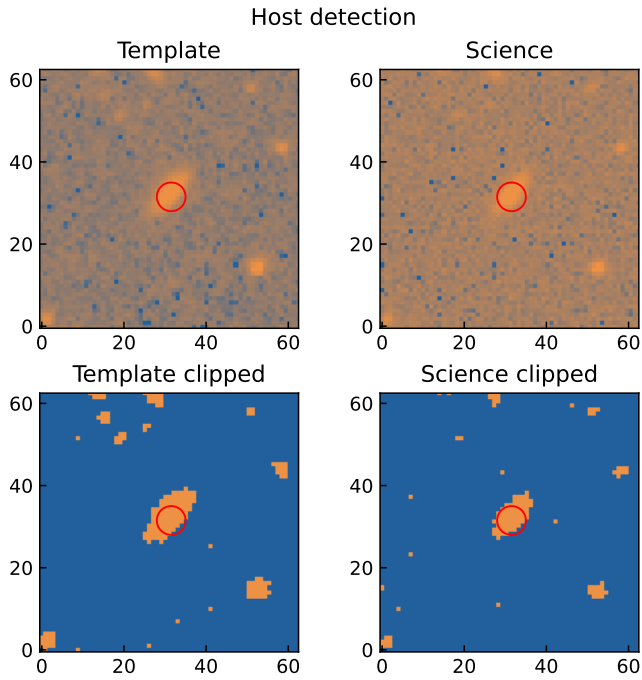


Fig. 1: Example of the *template* (left) and *science* (right) stamps for a transient associated with a host galaxy. The top row shows the original stamps and the bottom row shows the masks produced from sigma clipping. At the center of the stamps, we display a red circle of 7 pix radius that indicates the aperture radius of the associated photometry.

image acquisition process (Reyes-Jainaga et al. 2023). To guarantee a homogeneous sample, we removed any stamp whose size is smaller than the typical value. After applying these last conditions, we end with a total of 90 928 transients.

3. The ELEPHANT Pipeline

The pipeline analyses both the *science* and *template* stamps in parallel. Thus, a source is considered hostless if either its *template* or *science* stamps survives all filtering stages. In principle, the *template* image should suffice to detect the presence of a possible host, however, because of the *template* generation process (see Masci et al. 2019), some of them can suffer from transient contamination. In these cases, the transient would be detected as a source in the center of the *template* image, leading to the wrong detection of a host. Considering both the *template* and *science* stamps attenuates this issue. Below, we describe each step of the pipeline.

3.1. Stamp pre-processing

If a stamp contains pixels with missing or empty values, the pipeline estimates the probability density function (PDF) of the counts in the remaining pixels via Gaussian resampling using the `scipy.stats.gaussian_kde` Python method. The empty value is then replaced by randomly selected values from the resulting PDF, producing a homogenized sample where all images have the same number of valid pixels. Additionally, we use the full-width at half maximum (FWHM) of each stamp to estimate the image quality. In our sample, the FWHM can vary from $\text{FWHM} < 1.0''$ (a few cases) to $\text{FWHM} > 3.0''$, with a median value of $\text{FWHM} \sim 2.0''$. To select only the best available images

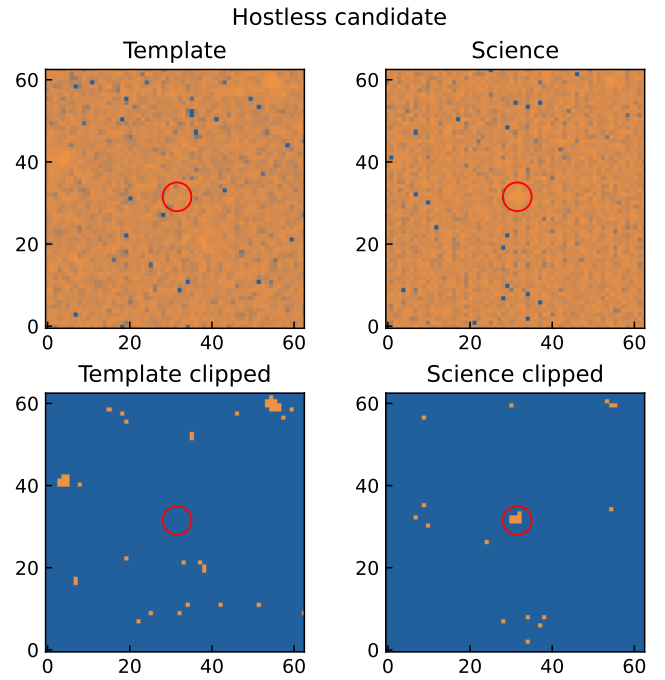


Fig. 2: Example of the *template* (left) and *science* (right) stamps of a hostless transient candidate. The top row shows the original stamps, and the bottom row shows the masks produced by sigma clipping. We can see that the *science* stamp shows a mask at the center of the stamp that is absent in the *template* stamp. The absence of a mask is considered as the absence of a host. At the center of the stamps, we display a red circle of 7 pix radius that indicates the aperture radius of the associated photometry.

representing each astrophysical source, all alerts associated with a given source are separated into 3 FWHM bins: $\text{FWHM} < 1.0''$, $1.0'' < \text{FWHM} < 2.0''$ and $\text{FWHM} > 2.0''$. The pipeline only considers the stamps in the smallest available FWHM bin for each source, discarding all others.

All selected stamps for a given object are then stacked by adopting the median count value in each pixel of the 63×63 cutout. This stacking process aids to enhance the images' signal-to-noise ratio (S/N), thereby improving the identification of potential hosts. Since the *science* stamps result from a single exposure, this process impacts them much more than their *template* counterparts. Nevertheless, this technique also serves to homogenize the effects of varying *templates* used throughout the lifespan of a given transient.

3.2. Segmentation masks

ELEPHANT uses sigma clipping to mask sources present in the stamps and uses those masks to detect the presence of a host galaxy. Sigma clipping is a typical method to detect outliers in astronomical images, usually used to remove the effect of defective pixels or cosmic rays by clipping out pixels above a given sigma threshold. The values of the clipped pixels can then be replaced with a mask or filled in with some characterization of the remaining image counts.

The ZTF alert package includes the aperture magnitude of the transient obtained from aperture photometry, calculated considering a 7-pixel radius aperture. We use this size as a reference for the maximum size of any detected transient. ELEPHANT

implements the `astropy.stats.sigma_clip`⁸ Python method considering $\sigma = 3$, median as the statistic to compute the clipping center value, and a maximum of ten iterations. As a result, any pixels above the selected median threshold are clipped. The clipped segments of the stamp are considered as the mask. If a mask bigger than 5 continuous pixels is found at the center of the *science* stamp but not at the center of the corresponding *template* stamp, or vice-versa, we flag the transient as a potential hostless candidate.

ELEPHANT utilizes the obtained masks to identify the position of the pixel closest to the center that corresponds to a detected neighboring mask, considering any masked pixel within a 7-pixel square as indicative of a neighbor's presence. Details on how the distance is computed can be found in Appendix A. Although we don't further use the distance information here, a future user could consider it to additionally assess the presence of a host. This could be useful when analyzing SN, as they could occur on the outskirts of their hosts. In such a case, a mask will not be found at the center of the stamp but close to it. In this context, what is considered to be close should be defined by the user. Another popular image segmentation software in astronomy is SExtractor; we decided not to use it here as it requires more resources than sigma clipping, and it also requires the pipeline to use out-of-memory processing; for further discussion on the use of SExtractor see Appendix B.

After applying sigma clipping, ELEPHANT retrieves 1669 hostless candidates. Fig. 1 and Fig. 2 show an example of a host detection and of the detection of a hostless candidate, respectively. Fig. 1 shows that the presence of a host galaxy at the center of the stamp is seen as a mask in the center of both the *template* and *science* stamps. On the other hand, Fig. 2 shows that a mask is present at the center of only one of the transient's stamps thus, it is flagged as a hostless candidate. Fig. 3 shows a spurious detection of a hostless candidate. In this case, the erroneous detection is driven by artifacts present on the *template* stamp.

3.3. Host categorization via Fourier power spectrum

To further examine the presence or absence of a host, if a transient is flagged as a hostless candidate by the sigma clipping method, ELEPHANT explores the Fourier space projections of the masked stamps. This strategy is reflective of methodologies previously applied to the classification of natural images across various landscapes (Balboa & Grzywacz 2003). By transforming the stamps into Fourier space, the pipeline is able to search for correlations in the background noise that can suggest the presence of a faint host, which would otherwise not be detected via the sigma clipping approach. This process involves calculating the medianized 1-dimensional power spectrum from the 2-dimensional Fourier transform of the images. The mathematical foundation of this method is laid out as follows: the Fourier transform, denoted by $F(u, v)$, of an image, $I(x, y)$, is calculated according to:

$$F(u, v) = \mathcal{F}\{I(x, y)\}, \quad (1)$$

where (x, y) represents the pixel coordinates and (u, v) the frequency domain coordinates. From this, the power spectrum, $P(u, v)$, is derived through the equation:

$$P(u, v) = |F(u, v)|^2. \quad (2)$$

⁸ https://docs.astropy.org/en/stable/api/astropy.stats.sigma_clip.html

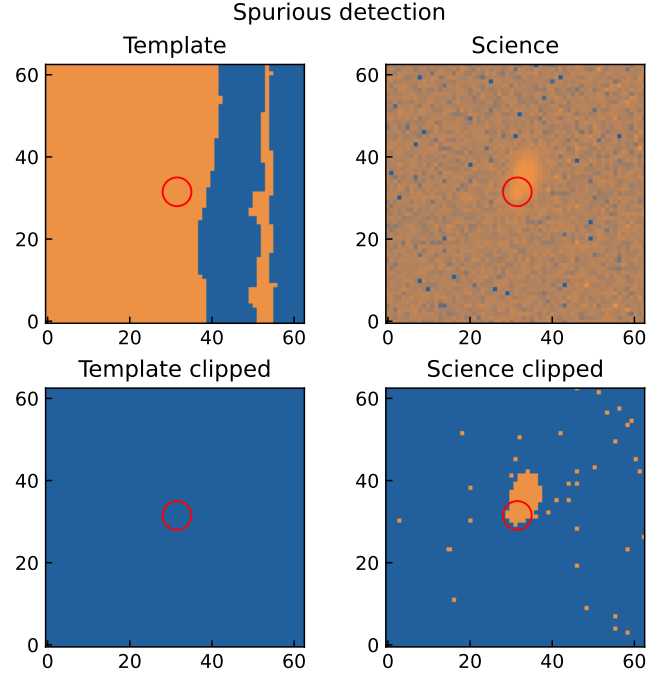


Fig. 3: Example of the *template* (left) and *science* (right) stamps of a spurious hostless candidate detection. The top row shows the original stamps and the bottom row shows the masks produced from sigma clipping. We can see that the erroneous detection is driven by artifacts present in the original *template* stamp. As a result, sigma clipped *template* shown on the bottom left panel shows no signal. At the center of the stamps, we display a red circle of 7 pix radius that indicates the aperture radius of the associated photometry.

The median power, $M(k)$, for each radial frequency $k = \sqrt{u^2 + v^2}$, is calculated by taking the median of the power values across all angular coordinates θ for a given power k :

$$M(k) = \text{median}\{P_k\}. \quad (3)$$

We assume that the power spectrum of an image containing even a faint host signal will distinguish itself from the power spectrum of another from which sources were removed and whose pixels have been randomly shuffled, and consequently does not contain any spatially coherent information to be extracted.

To explore this, we first compute the power spectrum of the original image. Subsequently, we use the masks resulted from sigma clipping and fill masked sections with random noise sampled from the pixel value distribution of the masked image itself. The images are then cropped to three distinct sizes: 7×7 , 15×15 , and 29×29 pixels, always with the center coinciding with the position of the transient. Afterwards, we randomly shuffle the pixel positions and the power spectrum is recalculated. This process is repeated 1000 times. The radially averaged 1D power spectrum of the original image is then compared to those of each shuffled iteration using the Wasserstein distance, $W(p, q)$:

$$W(p, q) = \inf_{\gamma \in \Pi(p, q)} \int_{X \times Y} \|x - y\| d\gamma(x, y), \quad (4)$$

which measures the distance between the p and q distributions. The presence of a host, even if weak, is suggested if the distances from the original image's power spectrum to those of the shuffled

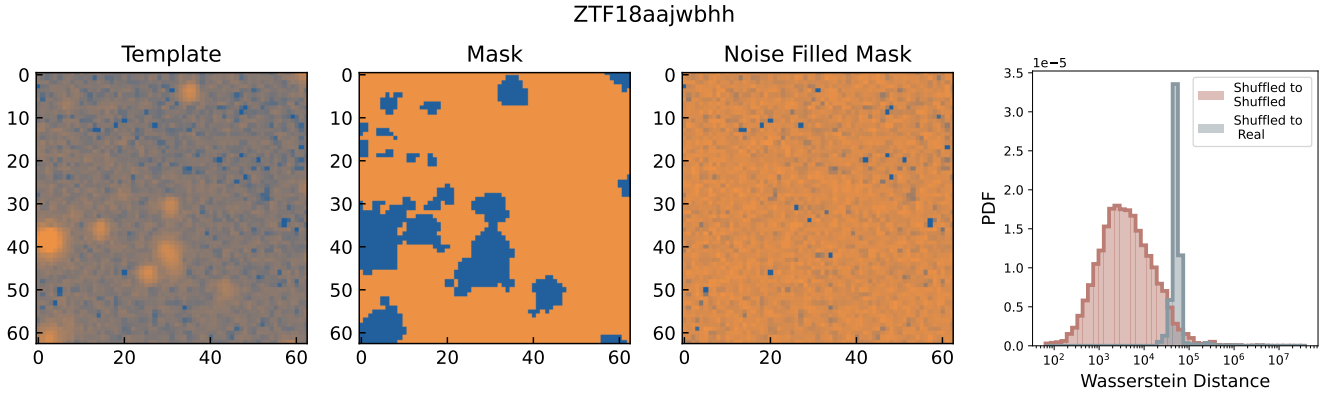


Fig. 4: Stages of the power spectrum analysis for a template with host (SN2017iuv / ZTF18aajwbhh). From left to right the panels show the template image, the mask and the mask populated with noise. The right-most panel shows the distribution of Wasserstein distances between the original template and shuffled noised masks (gray) and between random pairs of shuffled noised masks (rose). The distributions were generated using 1000 different shuffles of the noised masks within the central patch of 7×7 pixels.

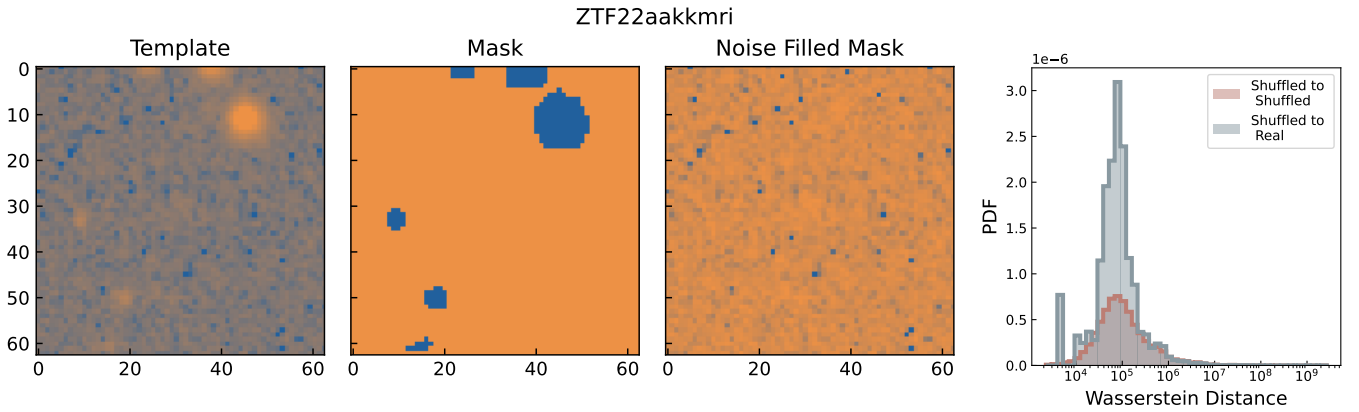


Fig. 5: Stages of the power spectrum analysis for a hostless template (SN2022knm / ZTF22aakkmri). Panel descriptions are equivalent to those described in Figure 4.

images are on average greater than the distances between the power spectra from shuffled images themselves (see right panel of Fig 4 for an example of distance distributions when a host is present, and Fig 5 for an example of the distance distributions for a hostless candidate).

This process yields a sample of 1000 distances for comparisons between the original image’s power spectrum and the power spectra of the shuffled images for each cutout size. The final step involves estimating the Kolmogorov-Smirnov (K-S) statistic to quantify the similarity between these two distributions of distances. The K-S statistic is calculated using the following equation:

$$D = \sup_{x \in \mathbb{R}} |S_1(x) - S_2(x)|, \quad (5)$$

where D quantifies the maximum discrepancy between the cumulative distribution functions (CDFs) of two distinct samples. Here, $S_1(x)$ represents the empirical cumulative distribution function (ECDF) for the first sample, which consists of the Wasserstein distances between the power spectrum of the original image and those derived from shuffled images. $S_2(x)$, on the other hand, corresponds to the ECDF of the second sample, namely the distribution of distances among the shuffled images themselves. We use D as a proxy for identifying the presence

of a faint host in all images which survived the sigma clipping selection.

4. Results

ELEPHANT combines 2 stages of filtering. All objects flagged as potential hostless candidates by the sigma clipping step (Section 3.2) were submitted to the power spectrum analysis (Section 3.3). This last stage attached to each object a K-S statistic value, D , which was constructed as a proxy indicating the presence of a faint host. We used a subset of visually inspected objects to define a selection cut threshold based on D (Section 4.1), and analyzed the results from imposing such a threshold on a subset of spectroscopically confirmed transients (Section 4.2).

4.1. D threshold for hostless candidates

After applying the segmentation mask module (see Section 3.2), ELEPHANT finds 1669 hostless candidates, 181 of these have an associated spectroscopic classification available on TNS. Fig. 6 compares the TNS classification (horizontal axis) against the classes found on SIMBAD (SN*_candidate, GinCl, SN and Unknown) or inferred via FINN classifiers (Microlensing candi-

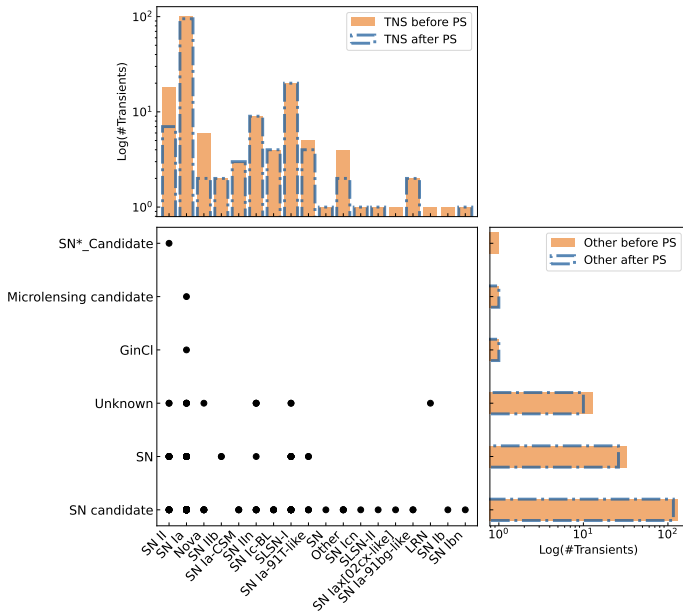


Fig. 6: Central panel: comparison between spectral classification reported on TNS (horizontal axis) and the classification reported by Fink obtained from other sources (vertical axis). The x and y axis side panels show the number of transients considered to be hostless by the sigma clipping method before applying the power spectrum (PS) analysis (orange), and the number of surviving hostless candidates after applying the PS analysis (blue).

date and SN candidate). We can see that most of these hostless candidates were classified as SN candidate by the ML classifiers, which is consistent with the final spectroscopic classification available on TNS.

The stamps associated with the 181 hostless candidates with a TNS classification were visually inspected using the Aladin sky atlas⁹ (Bonnarel et al. 2000). We were not able to visually identify a host for 118 candidates, thus we confirm them as hostless candidates. The remaining 63 events are considered to be contaminants. Figure 7 shows the distribution of the K-S statistic, D , for the three considered cropped cutout sizes (see Section 3.3), for both classes, confirmed hostless candidates and contaminants with host. We used the distribution of the hostless candidates to empirically define a threshold that would enclose a minimum of 75% of the hostless events. Table 1 shows the 75th percentile for each image size. Aiming at a low contamination level with 75% completeness, we chose to use the 15×15 pixel images and imposed a threshold of K-S statistic $D < 0.5$. Thus, we classify all objects with a K-S statistic below the threshold in either the *template* or the *science* image as hostless candidates. The last column of Table 1 shows the resulting contamination when the threshold is applied. We note that the output of ELEPHANT is the D value, and the user could employ a different threshold to select hostless candidates. In particular, the threshold could be further adjusted once more events are confirmed to be hostless.

4.2. Hostless sources on TNS

After applying the K-S D statistic threshold to all the events flagged as hostless candidates by the image segmentation method, we find a total of 1563 ZTF events that match our cri-

Image size (pix)	K-S threshold	Contamination (%)
7×7	0.25	27.01
15×15	0.50	25.97
29×29	0.90	27.33

Table 1: Kolmogorov-Smirnov statistic thresholds and corresponding contamination levels for different cutout sizes. The threshold was determined using only visually confirmed hostless objects with TNS classification and requiring completeness of 75%.

teria to be considered hostless candidates. We note that these events are flagged as hostless candidates because no extended source is found at the position of the transient at the center of the stamp. However, the transient could still be associated with a host that is either significantly off-center or that is dimmer than the limiting magnitude of the survey, which for ZTF is ~ 20.5 mag (Bellm et al. 2019). To define an event as truly hostless, user inspection is required. The retrieved number of hostless candidates represents $\lesssim 2\%$ of the analyzed extragalactic transients and $\lesssim 0.01\%$ of the number of transients processed by Fink between January/2022 and December/2023.

Among the hostless candidates retrieved after applying the K-S statistic threshold (Section 4.1), 154 have an associated spectroscopic classification available on TNS. As the threshold was applied to the complete sample produced by the sigma clipping procedure (Section 3.2), including those events for which a host was spotted via visual inspection (see Section 4.1), 40 of the 154 hostless candidates with a TNS classification actually have a host that can be identified visually. In other words, the TNS classified hostless candidates present a $\sim 26\%$ contamination, which is consistent with the value reported in Table 1. Table 2 the 154 events together with the reported classification. We can see that the most common class is Type Ia SNe, encompassing $\sim 67.5\%$ of events (considering all Type Ia subclasses). This is twice what was found by McCrum et al. (2015), but it is consistent with SNe Ia being predominant among hostless transients. The second most common class is SLSNe, which encompasses $\sim 14\%$ of the sample (considering both SLSNe I and SLSNe II). This is also consistent with the results of McCrum et al. (2015). In a few cases, a transient reported to TNS is associated to more than one ZTF identifier, Table 2 lists all of them, even if they are duplicated, this is because ELEPHANT only considers stamps associated to alerts, ignoring the associated coordinates. Inspecting the reasons for the duplicated ZTF identification is out of the scope of this paper.

The last column of Table 2 includes comments on some of the events. In particular, we see that a potential, usually faint, host has been reported on TNS for 11 events that we consider to be hostless. This is compatible with the contamination factor that we report above – further analysis is needed to confirm these associations. We also notice that eight of our hostless candidates were selected by the FLEET (“Finding Luminous and Exotic Extragalactic Transients” Gomez et al. 2020, 2023) pipeline as potentially luminous or exotic transients. In addition, five of our hostless candidates are part of the sample paper presented by Chen et al. (2023), that analyzes the characteristics of 78 SLSNe I. Moreover, three of the SNe reported in Table 2 were found in real-time by different groups, followed up, and studied in great detail due to their rare or anomalous nature. Below we provide further details on each of these events.

⁹ <https://aladin.cds.unistra.fr/>

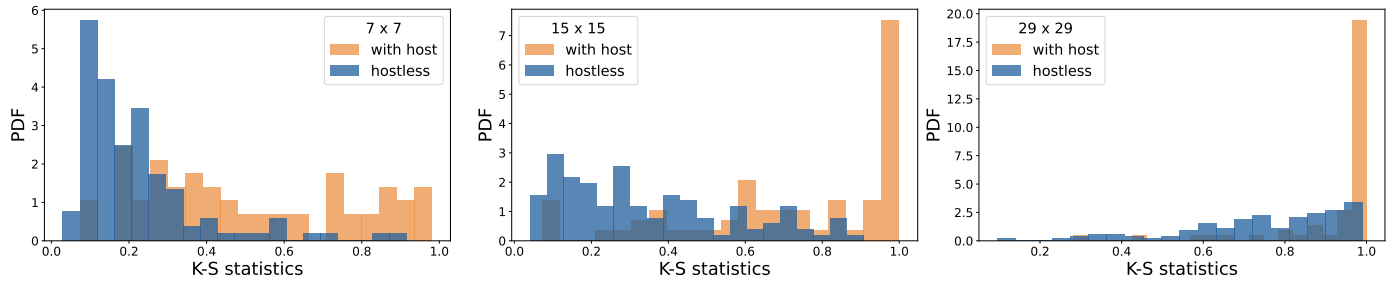


Fig. 7: Distributions of the Kolmogorov-Smirnov statistic for the 181 objects with TNS classifications. The two categories, with host (orange) and hostless (blue) were identified through visual inspection. Panels show distributions obtained through the power spectrum analysis (Section 3.3) for different image sizes.

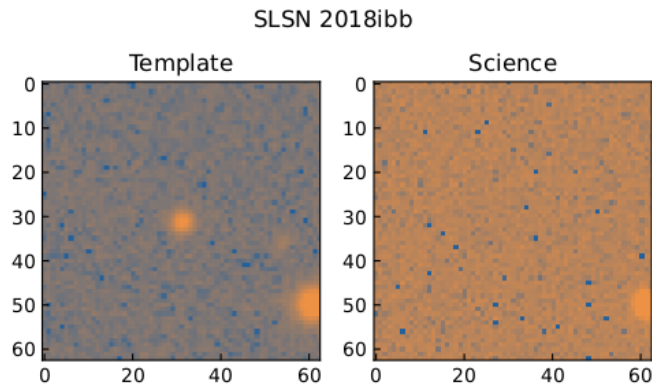


Fig. 8: Stacked *template* (left) and *science* (right) stamps for SLSN2018ibb (ZTF18acenqto, ZTF18adovhai).

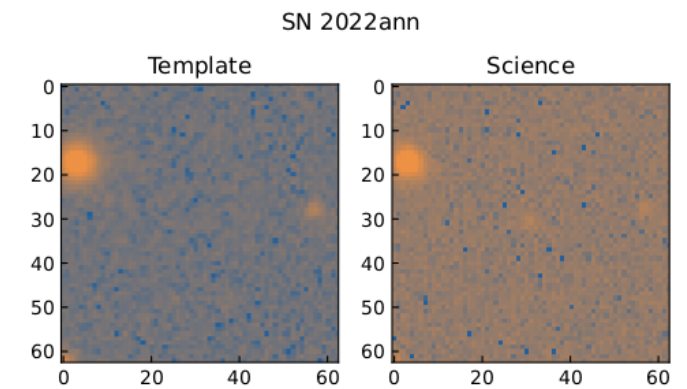


Fig. 10: Stacked *template* (left) and *science* (right) stamps for SN2022ann (ZTF22aaaihet).

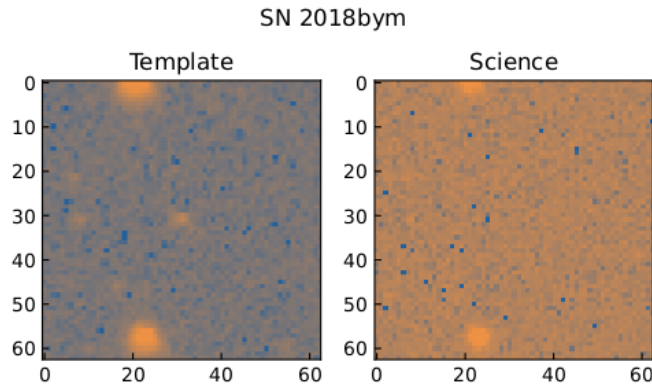


Fig. 9: Stacked *template* (left) and *science* (right) stamps for SN2018bym (ZTF18aapgrxo).

- SLSN 2018ibb was identified by Schulze et al. (2024) as the best pair-instability supernova (PISNe) candidate to date. It has been proposed that PISNe occur when instabilities produced by pair-production induce the thermonuclear explosion of the most massive stars ($140 M_{\odot} < M < 260 M_{\odot}$). Thus, it has been proposed that PISNe mark the explosive death of Population III stars, which could be indirectly studied through the characteristics of the observed explosion (e.g. Kasen et al. 2011; Gal-Yam 2012). Although SLSN 2018ibb is not hostless, it is associated with a faint ($m_R \sim 24.4$ mag Schulze et al. 2024) dwarf host, detected on 4- and 8-m class telescopes. Thus, for the purposes of

the ZTF alerts processed by our pipeline, the transient is expected to appear hostless. Figure 8 illustrates the interesting aspect which lead this object to be detected by our pipeline. It is a typical case of contaminated *template*, meaning that the *template* image was taken when the transient was bright, which results in a relatively lower central brightness in the *science* image. This result demonstrates the importance of considering both sets of stamps in parallel before a decision is made.

- SN 2018bym was studied by Lunnan et al. (2020) alongside three other SLSNe discovered by ZTF to examine the origin and diversity of these events. The authors find that SN 2018bym can be considered a classical SLSN I, and that it is associated with a faint ($m_r \sim 22.4$ mag) dwarf galaxy, for which they obtained deeper observations with the Canada–France–Hawaii Telescope (CFHT). This event is also a representative case of *template* contamination, where the hostless stamp is the *science* one (Figure 9).
- SN 2022ann was studied by Davis et al. (2023) as one of only five known SNe Icn. The early discovery of SN 2022ann enabled a detailed analysis of the progenitors of these rare objects. The authors find that SN 2022ann is associated with a faint dwarf host galaxy located in the lower end of the SN host galaxy luminosity distribution. Its stacked *template* and *science* stamps are shown in Figure 10.

The fact that ELEPHANT was able to identify such interesting sources while analyzing historical data demonstrates its potential in identifying similarly interesting objects when applied

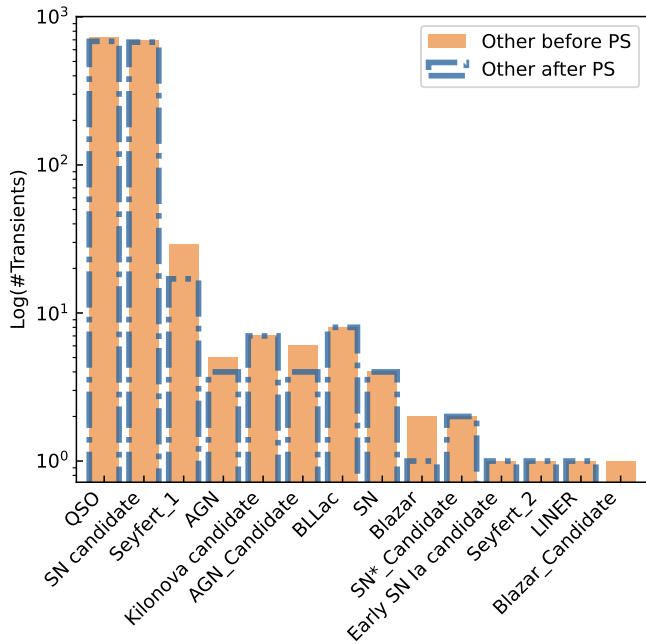


Fig. 11: Number of transients without a reported classification on TNS considered to be hostless by the sigma clipping method before applying the power spectrum (PS) analysis (orange), and the number of surviving hostless candidates after applying the PS analysis (blue).

to more recent alerts. We are currently working on such an investigation and, in parallel, integrating ELEPHANT to Fink. Preliminary results are encouraging and will be reported in a subsequent work. We also anticipate that, among other applications, the pipeline can serve as a powerful tool to identify SNe potentially associated to dwarf host galaxies (e.g. Taggart & Perley 2021).

The classification distribution of the hostless candidates that do not have a class available on TNS is shown in Fig. 11. The classification associated with these events is mainly obtained from cross-match with SIMBAD or inferred using a ML classifier. We find that $\sim 49\%$ of these events are QSOs, which belong to the family of AGN and, thus, would be associated with a host by definition. However, hostless QSOs have been found before (e.g. Magain et al. 2005; Kemper et al. 2010). Although many of the QSOs in our sample of hostless candidates may be associated with a faint, undetected host, ELEPHANT can be used to perform systematic searches of hostless QSOs. The other dominant class in this sample is “SN candidate”, $\sim 48\%$ of the sample is associated with this ML-based classification. As mentioned above, ELEPHANT only considers ZTF stamps associated to individual alerts, however, some events seems to be associated to multiple ZTF identifiers, when this occurs we considered all of the different identifications to be hostless candidates. An interesting case is that of AT 2024dum, this object was found to be a hostless candidate and is associated to three ZTF alerts: ZTF23aabyzn, ZTF23aaiyhen and ZTF23abkiray. AT 2024dum has been reported to be a fast-moving star (see report¹⁰ by Shumkov et al. 2024), which could explain the multiplicity of ZTF identifiers.

¹⁰ <https://www.wis-tns.org/object/2024dum>

5. Conclusions

We developed the ELEPHANT pipeline, which processes stamps delivered by the ZTF alert stream and automatically detects hostless transient candidates. The pipeline (see Section 3) returns stacked *science* and *template* cutouts together with the number of stamps that were used to produce them, a boolean that indicates whether the transient is a hostless candidate based on the segmentation mask analysis (see Section 3.2), the distance to the closest mask in pixels and the associated K-S D statistic obtained from 7×7 , 15×15 and 29×29 pixel square sub-cutouts (see Section 3.3).

In this work, we define a threshold on the K-S D statistic that is used to flag a transient as a hostless candidate (see Section 4). However, future users can use the output values to implement different selection cuts specific to their science case. The automatic detection of hostless transients has many potential applications that include but are not limited to:

1. Identification of transients associated with dwarf and/or dim galaxies to study their characteristics and environments;
2. Identification of AGNs associated with low-mass galaxies to study their impact on galaxy evolution;
3. Search of sources that have been ejected from their host galaxies to study intra-cluster stellar populations;
4. Selection of SNe Ia and/or SLSNe, as they seem to be predominant among the hostless candidates that have a reported class on TNS;
5. Compilation of hostless candidates as training sets to improve ML classifiers.

ELEPHANT will be included in the Fink broker to allow the real-time detection of hostless candidates and also the retrieval of archival potentially hostless events. Recently, Qin et al. (2024) performed an statistical analysis of the environments of 161 hostless SNe reported to TNS since 2016. They find that their sample is dominated by SNe Ia and SLSNe, which is in agreement with our findings. ELEPHANT is a useful tool to gather hostless events for similar statistical environmental analyses of different types of SNe. In addition, it can be used to systematically select hostless candidates for classification to increase the number of spectroscopically classified hostless transients to be considered in future population analyses.

The methods we use here are completely transferable to any dataset by scaling the sizes of the considered stamps. In particular, once the Fink broker starts ingesting LSST alerts, we could test and tune ELEPHANT as a tool for finding hostless candidates within the LSST alert stream. LSST is an 8-m class telescope that will have a limiting magnitude of ~ 25 mag in optical bands (LSST Science Collaboration et al. 2009), which makes it much deeper than the current wide-field surveys. Thus, a big fraction of the events that we flag as hostless candidates here may have a visible host in the LSST stamps. Consequently, if an LSST stamp is flagged to be a hostless by ELEPHANT the chances are that the transient is either part of the intra-cluster medium or, it is associated to hosts dimmer than any detected so far. We can only speculate that the hostless transients detected by LSST will be extraordinarily anomalous providing unprecedented insights to the transient sky, with the study of their environments only being possible by using other 8-m class telescopes or by the next generation of large telescopes such as the Giant Magellan Telescope (Johns et al. 2012) and the Extremely Large Telescope (Gilmozzi & Spyromilio 2007). In this context, automatic pipelines tailored for specific science cases, such as ELEPHANT will play a central role in the process of transient characterization and optimization of follow-up resources.

Table 2: Hostless candidates with associated spectroscopic classification in TNS.

	IAU Name	ZTF Name	R.A. [J2000]	Dec. [J2000]	Class	Confirmed	Comments
1	SN 2016ieq	ZTF19abkaxlf	21:22:25.18	-11:56:54.82	SNIIIn	×	
2	SN 2017iuu	ZTF18aajwbhh	06:27:40.06	47:29:45.51	SNIIa	✓	Several potential hosts, no redshift info.
3	SN 2018fd	ZTF18adoeywv	09:10:36.36	35:43:18.39	SLSN-I	×	
4	SN 2018gj	ZTF18aaxljll	16:32:02.27	78:12:40.96	SNII	×	
5	SN 2018hh	ZTF18aaajfsd	12:13:41.40	28:26:39.92	SNIIa	×	
6	SN 2018kl	ZTF18aaacdnd	09:09:37.99	48:39:39.95	SNIIa	✓	Potential host association on TNS.
7	SN 2018mc	ZTF18aatpnrf	18:01:00.89	61:41:46.76	SNIIb	×	
8	SN 2018vx	ZTF18adkgyxe	14:43:10.45	17:28:16.76	SNIIa-91T-like	×	Potential host association on TNS.
9	SN 2018vx	ZTF18aaznlwl	14:43:10.44	17:28:16.88	SNIIa-91T-like	×	
10	SN 2018yc	ZTF18aabqgnb	11:52:45.48	37:51:15.44	SNIIa	×	
11	SN 2018aae	ZTF18aaaiscil	12:21:34.21	55:34:27.98	SNIIa	✓	Faint host in Gaia.
12	SN 2018bym	ZTF18aapgrxo	18:43:13.41	45:12:28.23	SLSN-I	✓	Lunnan et al. (2020); Chen et al. (2023).
13	SN 2018cog	ZTF18aaxtdcm	15:26:11.95	06:21:25.87	SNIIa	✓	
14	SN 2018cxa	ZTF18abfylqx	22:28:34.59	11:37:05.55	SLSN-I	×	
15	SN 2018eem	ZTF18absoghh	23:36:01.41	18:41:07.06	SNII	×	
16	SN 2018fcg	ZTF18admasii	21:09:36.77	33:28:59.43	SLSN-I	×	
17	SN 2018fer	ZTF18abtvtb	20:33:05.24	-20:51:24.43	SNIIb	✓	
18	SN 2018ffj	ZTF18abslpjy	02:30:59.80	-17:20:26.84	SLSN-I	✓	Garcia-Zamora et al. (2018).
19	SN 2018ftd	ZTF18abotdef	02:01:16.09	-01:13:26.91	SNIIa	✓	
20	SN 2018fus	ZTF18abskoyh	21:02:31.29	-05:37:30.08	SNII	×	
21	SN 2018gck	ZTF18abskzjm	00:50:56.6	03:29:55.20	SNIIa	✓	
22	SN 2018gck	ZTF18adnfmkzf	00:50:56.61	03:29:55.00	SNIIa	✓	
23	SN 2018gkz	ZTF18abvgjyl	07:58:11.55	19:31:07.99	SLSN-I	×	Chen et al. (2023).
24	SN 2018htb	ZTF18acdqmrx	04:37:30.67	20:16:55.70	SNIIa	×	
25	SN 2018ibb	ZTF18acenqto	04:38:56.94	-20:39:44.06	SLSN-I	✓	Schulze et al. (2024); Chen et al. (2023).
26	SN 2018ibb	ZTF18adovhai	04:38:56.95	-20:39:43.93	SLSN-I	✓	
27	SN 2018icz	ZTF18accngfb	10:03:14.82	15:04:42.87	SNIIa	✓	Gaia hostless candidate.
28	SN 2018imd	ZTF18acydvjn	12:48:24.97	-05:47:39.10	SNIIa	×	
29	SN 2018imq	ZTF18acepwhb	11:34:45.61	77:03:09.99	SNIIa	✓	
30	SN 2018jeo	ZTF18aczddnw	09:04:36.91	-19:47:09.60	SNIIa	×	
31	SN 2018lzw	ZTF18abrzcbb	07:39:32.76	27:44:02.62	SLSN-I	✓	Chen et al. (2023).
32	SN 2018lzx	ZTF18abszecz	22:29:27.23	13:10:39.96	SLSN-I	✓	Chen et al. (2023).
33	SN 2019aatt	ZTF19abszdld	01:21:21.63	30:17:03.52	SNIIa	×	
34	SN 2020jhs	ZTF20aayvmyh	09:28:14.10	25:40:13.39	SNIIIn	✓	
35	SN 2021rll	ZTF21abiwpjm	13:45:21.99	26:45:00.72	SNIIIn	✓	Faint host in Pan-STARRS.
36	SN 2022aj	ZTF22aaafohf	14:56:08.32	-27:45:37.53	SNIIa	✓	Gaia hostless candidate.
37	SN 2022aj	ZTF22aaausrb	14:56:08.31	-27:45:37.58	SNIIa	✓	Gaia hostless candidate.
38	SN 2022ait	ZTF22aaaiykj	10:30:26.97	07:10:21.19	SNIIa	✓	
39	SN 2022ann	ZTF22aaaihet	10:17:29.66	-02:25:35.40	SNIIcn	✓	Davis et al. (2023).
40	SN 2022are	ZTF22aaahull	09:59:07.08	-18:11:02.83	SNIIa	✓	
41	SN 2022bic	ZTF22aaagvyp	08:39:08.93	60:59:16.25	SNIIa	✓	
42	SN 2022cjb	ZTF22aaafavg	11:34:34.66	31:02:40.71	SNIIa	✓	
43	SN 2022ddh	ZTF22aabtyli	10:28:15.83	06:34:47.31	SNIIa	×	
44	SN 2022dld	ZTF22aabwvot	14:06:16.60	13:29:30.89	SNIIa	✓	FLEET Candidate.
45	SN 2022fjx	ZTF22aadlmgg	10:43:30.16	19:04:58.70	SNIIa-91bg-like	✓	
46	SN 2022ful	ZTF22aadeuwu	19:20:10.68	50:23:42.41	SLSN-I	✓	Gaia hostless candidate.
47	SN 2022ful	ZTF22aafumyr	19:20:10.67	50:23:42.40	SLSN-I	✓	Gaia hostless candidate.
48	SN 2022gkv	ZTF22aafctmp	15:57:51.12	29:55:10.78	SNIIa	✓	
49	SN 2022gkv	ZTF22aadetzs	15:57:51.12	29:55:10.82	SNIIa	✓	
50	SN 2022gsp	ZTF22aadqkqp	14:53:08.28	13:59:57.53	SNIIa	×	
51	SN 2022hdn	ZTF22aagbxrb	15:00:09.14	36:07:13.14	SNIIc-BL	✓	Potential host association on TNS.
52	SN 2022huk	ZTF22aahaasc	10:14:12.85	-23:41:17.10	SNIIa	✓	
53	SN 2022hwk	ZTF22aagzbux	12:45:59.22	59:15:37.04	SNIIIn	×	

54	SN 2022igq	ZTF22aahecwj	13:56:52.02	19:07:01.66	SN Ia	✓	
55	SN 2022ihz	ZTF22aahgxd	09:42:48.23	-03:36:25.48	SN Ia-91bg-like	✓	
56	SN 2022irt	ZTF22aahhubz	12:27:12.57	00:55:40.00	SN Ia	✓	
57	SN 2022jii	ZTF22aaizxqg	14:54:31.30	04:19:52.83	SN Ia	✓	Potential host association on TNS.
58	SN 2022jnr	ZTF22aajhtpy	15:02:39.48	17:14:23.45	SN Ia	×	
59	SN 2022jzt	ZTF22aakanzk	13:43:12.79	48:23:10.82	SN Ia	✓	Potential host association on TNS.
60	SN 2022knm	ZTF22aakkmri	13:25:04.36	-24:39:24.94	SN Ia	✓	
61	SN 2022llq	ZTF22aalmrqp	12:03:16.55	51:49:54.24	SN Ia	✓	
62	SN 2022lxd	ZTF22aaljlzq	17:36:38.67	61:33:18.66	SLSN-I	✓	
63	SN 2022mjk	ZTF22aapuake	01:25:41.36	01:45:41.27	SN Ia	✓	
64	SN 2022nab	ZTF22aaoibrbd	18:38:57.89	48:23:04.86	SN Ia	✓	
65	AT 2022nci	ZTF22aaombjf	00:46:33.41	41:45:35.15	Nova	✓	
66	SN 2022ncx	ZTF22aaogwbd	12:08:13.50	66:38:24.84	SN Ia-91T-like	✓	
67	SN 2022ojm	ZTF22aapjqpn	23:37:46.03	40:05:07.96	SLSN-I	✓	
68	SN 2022orr	ZTF22aasaapb	15:50:58.27	68:35:07.80	SN Ia	✓	
69	SN 2022owf	ZTF22aaszlph	23:26:09.97	27:42:02.97	SN Ia	✓	
70	SN 2022rfn	ZTF22abahblc	19:11:28.98	-17:11:07.59	SN Ia	×	
71	SN 2022rhl	ZTF22aasoali	19:20:44.21	46:52:54.75	SN IIn	✓	
72	SN 2022rpm	ZTF22abamxcl	02:01:11.36	-05:51:59.41	SN	✓	
73	SN 2022sff	ZTF22abdibiz	07:56:05.03	33:28:18.38	SN Ia	×	
74	SN 2022tis	ZTF22abepfmn	21:10:35.86	-09:30:14.39	SN II	✓	
75	SN 2022uhk	ZTF22abfwchw	18:50:17.25	75:27:59.88	SN II	✓	
76	SN 2022uot	ZTF22abfyvhf	05:37:10.51	68:34:31.96	SN IIn	✓	
77	SN 2022uwh	ZTF22abfxmvf	23:53:37.16	11:22:58.08	SN Ia	✓	
78	SN 2022wlm	ZTF22abjafpr	05:56:46.63	48:06:20.85	SN Ic-BL	✓	
79	SN 2022wpp	ZTF22abjrpmv	16:41:49.91	15:15:45.35	SN Ia	✓	
80	SN 2022wuw	ZTF22ablcyyb	16:26:19.28	80:28:41.33	SN Ia	✓	
81	SN 2022wuy	ZTF22ablhlnd	06:44:23.34	32:14:53.21	SN Ia	✓	
82	SN 2022xjl	ZTF22abmpqbq	23:57:11.78	05:36:17.35	SN Ia	✓	
83	SN 2022xxn	ZTF22abmxtqr	01:18:56.59	-12:57:44.93	SN Ia	✓	
84	SN 2022ycr	ZTF22abnwvyc	21:23:27.18	-18:06:13.85	Other	×	
85	SN 2022ydl	ZTF22abnqzle	22:40:04.43	-06:38:28.35	SN Ia	✓	
86	SN 2022yig	ZTF22aboaiim	05:20:21.53	-20:54:41.61	SN Ia	×	
87	SN 2022yru	ZTF22aboixdd	10:27:28.41	70:59:02.23	SN Ia	×	
88	AT 2022zzj	ZTF22ablttcw	00:41:25.73	40:44:23.34	Nova	×	Potential host association on TNS.
89	SN 2022aahy	ZTF22abtsypf	06:58:56.24	39:38:06.90	SN IIn	×	
90	SN 2022aahz	ZTF22abtotgu	12:25:54.64	06:45:02.96	SN Ia	✓	
91	SN 2022abtm	ZTF22abvngdr	23:03:54.16	15:46:19.84	SLSN-I	✓	
92	SN 2022acfw	ZTF22abzakdd	13:21:06.78	27:54:53.79	SN Ia	×	
93	SN 2022acmr	ZTF22abyhqkt	02:02:39.45	-07:02:22.67	SN Ia	✓	
94	SN 2022acsx	ZTF22abyunkpz	06:12:59.10	68:48:45.39	SLSN-I	✓	Faint host in DESI Legacy Surveys DR10.
95	SN 2022adbl	ZTF22abyuoan	07:57:29.24	62:25:39.25	SN Ia	×	
96	SN 2022adrs	ZTF22abzbyyw	00:27:08.37	-24:53:50.88	SN Ia	✓	
97	SN 2022advb	ZTF22abyznto	09:40:44.48	05:10:21.13	SN Ia	✓	
98	SN 2022adxq	ZTF22abzvyku	03:27:24.99	-17:37:50.35	SN Ia	✓	
99	SN 2023ha	ZTF23aaajtqn	09:19:32.46	-01:11:34.62	SN Ia	×	
100	SN 2023ael	ZTF23aaawbsy	17:14:41.46	66:51:22.60	SN Ia	✓	Gaia hostless candidate.
101	SN 2023aiw	ZTF23aaawcvx	16:31:09.06	39:47:20.59	SN Ia	×	
102	SN 2023ayq	ZTF23aaazegi	13:24:05.23	-03:33:41.04	SN Ia-CSM	✓	
103	SN 2023bee	ZTF23aabtgej	08:56:11.63	-03:19:32.05	SN Ia	×	
104	SN 2023cpq	ZTF23aacdnjz	17:29:20.16	14:11:04.51	SN Ia-CSM	✓	FLEET Candidate.
105	SN 2023cze	ZTF23aadbswn	15:05:05.39	28:28:52.45	SN Ia	✓	
106	SN 2023ebb	ZTF23aadruma	11:24:34.69	46:53:37.14	SN II	✓	
107	SN 2023erb	ZTF23aaejvzv	16:37:54.80	43:23:08.60	SN Ia	×	
108	SN 2023exi	ZTF23aaelzdb	07:04:14.64	67:37:32.53	SN Ia	✓	
109	SN 2023ffw	ZTF23aaemgto	11:35:12.53	-13:30:47.90	SN Ia	✓	
110	SN 2023fvf	ZTF23aafggjj	13:20:51.42	15:17:37.91	SN Ia	×	
111	SN 2023gav	ZTF23aafthouh	10:47:18.35	-05:07:22.75	SN Ia	✓	FLEET Candidate.
112	SN 2023ger	ZTF23aagaiju	10:57:13.46	42:58:50.06	SN Ia	✓	
113	SN 2023ghq	ZTF23aagunkc	15:58:13.05	08:54:24.99	Other	✓	

114	SN 2023hoz	ZTF23aagdbbv	16:18:21.55	01:31:43.41	SLSN-I	✓	FLEET Candidate.
115	SN 2023hrn	ZTF23aaiyexs	11:08:35.07	04:48:52.09	SN Ia	×	
116	SN 2023huv	ZTF23aafmjbx	13:29:03.66	-10:25:29.42	SN IIIn	✓	FLEET Candidate.
117	SN 2023iar	ZTF23aajenxf	13:31:36.14	04:55:21.32	SN Ia	✓	
118	SN 2023ifa	ZTF23aajhtuu	09:33:34.73	51:36:54.11	SN Ibn	×	
119	SN 2023iwy	ZTF23aakmewi	18:00:18.62	26:24:32.04	SN Ic-BL	✓	
120	SN 2023jsb	ZTF23aamfmqm	21:49:58.44	14:09:24.71	SN Ia	✓	
121	SN 2023jvu	ZTF23aamqonh	16:38:00.64	55:24:18.30	SN Ia	×	
122	SN 2023khp	ZTF23aamsekn	00:17:56.20	23:59:03.33	SN Ia-CSM	✓	
123	SN 2023kkh	ZTF23aanuvih	18:49:05.23	45:07:10.91	SN Ia	✓	
124	SN 2023kki	ZTF23aamxeoe	16:53:18.11	37:41:23.52	SN IIIn	✓	
125	SN 2023kvk	ZTF23aanukvi	20:02:32.44	-05:05:16.88	SN Ia	✓	
126	SN 2023mhj	ZTF23aapvrkk	00:00:42.10	-12:14:12.51	SN Ia	✓	
127	SN 2023mir	ZTF23aaqfdbv	22:40:59.46	-05:04:15.74	SN Ia	✓	
128	SN 2023mit	ZTF23aaqjuux	16:28:18.62	23:10:56.15	SN Ia	✓	
129	SN 2023nbf	ZTF23aawcygl	13:08:46.93	49:24:08.67	SN Ia	×	
130	SN 2023pjx	ZTF23aaxyawz	01:31:25.59	12:24:31.35	SN Ia	✓	
131	SN 2023qpe	ZTF23aazrtdy	23:40:15.79	15:27:50.97	SN Ia	✓	Potential host association on TNS.
132	SN 2023qrz	ZTF23aaznifc	21:55:14.72	-17:35:31.55	SN Ia	✓	
133	SN 2023qvl	ZTF23aawhcbj	15:50:08.30	53:39:37.03	SLSN-I	✓	FLEET Candidate.
134	SN 2023qzo	ZTF23abaderr	01:35:05.20	-22:40:37.84	SN Ia	×	
135	SN 2023rbt	ZTF23abaslfm	01:46:31.43	11:51:55.34	SN Ia	✓	
136	SN 2023rfg	ZTF23abavpyk	23:31:06.17	-27:00:56.44	SN Ia	✓	
137	SN 2023slt	ZTF23abbsfxp	03:34:04.42	-21:54:21.92	SN Ia	✓	FLEET candidate.
138	SN 2023spg	ZTF23abcufxh	00:11:56.30	-07:46:19.56	SN Ia	✓	
139	SN 2023svf	ZTF23abcqzvm	16:44:05.26	30:18:09.99	SN Ia	✓	
140	SN 2023syg	ZTF23abdynfn	20:49:40.99	-14:43:26.57	SN Ia	✓	
141	SN 2023szi	ZTF23aaznlgf	22:19:56.03	25:54:56.17	SLSN-I	✓	FLEET Candidate.
142	SN 2023tqm	ZTF23abgvtxr	07:57:28.61	51:07:23.93	SN Ia	✓	
143	SN 2023upt	ZTF23abjqxbe	04:28:27.38	-17:53:27.26	SN Ia	✓	
144	SN 2023uqu	ZTF23abijopy	17:47:47.83	64:20:57.31	SN Ia	✓	Potential host association on TNS.
145	SN 2023vkz	ZTF23ablspnz	08:28:36.18	57:12:31.86	SN II	✓	
146	SN 2023wml	ZTF23aboebgh	11:39:08.69	-11:14:57.92	SLSN-I	✓	
147	SN 2023wrn	ZTF23aboemfi	23:31:53.52	22:39:30.74	SN Ia	✓	
148	SN 2023wtq	ZTF23abochfb	01:21:55.68	-03:46:19.95	SN Ic-BL	✓	
149	SN 2023xjs	ZTF23abpqklj	02:26:34.56	-19:10:26.42	SN Ia	✓	Faint host in Pan-STARRS.
150	SN 2023yqq	ZTF23abryfga	22:56:04.96	19:34:56.71	SN Ia	✓	
151	SN 2023yti	ZTF23absflyh	02:06:22.20	-18:19:06.12	SN Ia	✓	
152	SN 2023zeq	ZTF23abqygjv	01:08:54.20	-20:38:24.23	SLSN-II	✓	
153	SN 2023zjv	ZTF23absbyol	07:14:10.46	36:09:52.82	SN Ia	×	
154	SN 2023aajn	ZTF23abvbwys	03:41:33.85	-02:46:50.01	SN Ia-91T-like	✓	

First column presents the IAU name of each object. The second column shows the corresponding ZTF internal name. The third and fourth columns show right ascension and declination, respectively. Column five shows the classification available on TNS. In the sixth column we indicate whether we can visually confirm the lack of an obvious host associated with the transient. In the last column we add additional remarks about certain events.

Acknowledgements

We thank Julien Peloton for assistance in retrieving data from FINK. P.J.P. acknowledges support from the European Research Council (ERC) under the European Union’s Horizon Europe research and innovation program (grant agreement No. 10104229 – TransPIre). EEH is supported by a Gates Cambridge Scholarship (#OPP1144). This work is a result of the COIN Residence Program #7¹¹, held in Lisbon, Portugal, from 9 to 16 September 2023 and supported by the Portuguese Fundação para a Ciência e a Tecnologia (FCT) through the Strategic Programme UIDP/FIS/00099/2020 and UIDB/FIS/00099/2020 for CENTRA. The Cosmostatistics Initiative (COIN, <https://cosmostatistics-initiative.org/>) is an international network of researchers whose goal is to foster interdisciplinarity inspired by astronomy. This research has made use of the SIMBAD database, operated at CDS, Strasbourg, France. This research has made use of “Aladin sky atlas” developed at CDS, Strasbourg Observatory, France. This work made use of Astropy (<http://www.astropy.org>) a community-developed core Python package and an ecosystem of tools and resources for astronomy (Astropy Collaboration et al. 2013, 2018, 2022). The ELEPHANT icon was taken from <https://icons8.com>. The color palette used in this work was inspired by “The Temptation of St. Anthony” by Salvador Dali, 1946.

Data Availability

The data used here can be accessed via the FINK data transfer service: <https://fink-portal.org/download>. The ELEPHANT pipeline is publicly available on github: https://github.com/COINtoolbox/extragalactic_hostless.

References

- Astropy Collaboration, Price-Whelan, A. M., Lim, P. L., et al. 2022, *ApJ*, 935, 167
- Astropy Collaboration, Price-Whelan, A. M., Sipőcz, B. M., et al. 2018, *AJ*, 156, 123
- Astropy Collaboration, Robitaille, T. P., Tollerud, E. J., et al. 2013, *A&A*, 558, A33
- Balboa, R. M. & Grzywacz, N. M. 2003, *Vision Research*, 43, 2527
- Baldwin, J. A., Phillips, M. M., & Terlevich, R. 1981, *PASP*, 93, 5
- Bellm, E., Blum, R., Graham, M., et al. 2019, *LDM-612*, Plans and Policies for LSST Alert Distribution, <https://ls.st/ldm-612>
- Bellm, E. C., Kulkarni, S. R., Graham, M. J., et al. 2019, *PASP*, 131, 018002
- Bertin, E. & Arnouts, S. 1996, *A&AS*, 117, 393
- Biswas, B., Ishida, E. E. O., Peloton, J., et al. 2023, *A&A*, 677, A77
- Bonnarel, F., Fernique, P., Bienaymé, O., et al. 2000, *A&AS*, 143, 33
- Chen, Z. H., Yan, L., Kangas, T., et al. 2023, *ApJ*, 943, 41
- Davis, K. W., Taggart, K., Tinyanont, S., et al. 2023, *MNRAS*, 523, 2530
- Drout, M. R., Chornock, R., Soderberg, A. M., et al. 2014, *ApJ*, 794, 23
- Ducoin, J. G., Corre, D., Leroy, N., & Le Floch, E. 2020, *MNRAS*, 492, 4768
- Filippenko, A. V. 1997, *ARA&A*, 35, 309
- Förster, F., Cabrera-Vives, G., Castillo-Navarrete, E., et al. 2021, *AJ*, 161, 242
- Gaia Collaboration, Prusti, T., de Bruijne, J. H. J., et al. 2016, *A&A*, 595, A1
- Gal-Yam, A. 2012, in *Death of Massive Stars: Supernovae and Gamma-Ray Bursts*, ed. P. Roming, N. Kawai, & E. Pian, Vol. 279, 253–260
- Garcia-Zamora, E. M., Hernandez-Garcia, A., Mallorquin, M., et al. 2018, *The Astronomer’s Telegram*, 12344, 1
- Gillanders, J. H., Rhodes, L., Srivastav, S., et al. 2024, *arXiv e-prints*, arXiv:2404.10660
- Gilmozzi, R. & Spyromilio, J. 2007, *The Messenger*, 127, 11
- Gomez, S., Berger, E., Blanchard, P. K., et al. 2023, *ApJ*, 949, 114
- Gomez, S., Berger, E., Blanchard, P. K., et al. 2020, *ApJ*, 904, 74
- Graham, M. L., Sand, D. J., Zaritsky, D., & Pritchett, C. J. 2015, *ApJ*, 807, 83
- Hambleton, K. M., Bianco, F. B., Street, R., et al. 2023, *PASP*, 135, 105002
- Ho, A. Y. Q., Perley, D. A., Beniamini, P., et al. 2020, *ApJ*, 905, 98

- Johns, M., McCarthy, P., Raybould, K., et al. 2012, in *Society of Photo-Optical Instrumentation Engineers (SPIE) Conference Series*, Vol. 8444, Ground-based and Airborne Telescopes IV, ed. L. M. Stepp, R. Gilmozzi, & H. J. Hall, 84441H
- Kankare, E., Kotak, R., Mattila, S., et al. 2017, *Nature Astronomy*, 1, 865
- Kasen, D., Woosley, S. E., & Heger, A. 2011, *ApJ*, 734, 102
- Kemper, F., Woods, P. M., Antoniou, V., et al. 2010, *PASP*, 122, 683
- Leoni, M., Ishida, E. E. O., Peloton, J., & Möller, A. 2022, *A&A*, 663, A13
- LSST Science Collaboration, Abell, P. A., Allison, J., et al. 2009, *arXiv e-prints*, arXiv:0912.0201
- Lunnan, R., Yan, L., Perley, D. A., et al. 2020, *ApJ*, 901, 61
- Magain, P., Letawe, G., Courbin, F., et al. 2005, *Nature*, 437, 381
- Martin, J. C. 2006, *AJ*, 131, 3047
- Masci, F. J., Laher, R. R., Rusholme, B., et al. 2019, *PASP*, 131, 018003
- Matheson, T., Stubens, C., Wolf, N., et al. 2021, *AJ*, 161, 107
- McCrum, M., Smartt, S. J., Rest, A., et al. 2015, *MNRAS*, 448, 1206
- Möller, A. & de Boissière, T. 2020, *MNRAS*, 491, 4277
- Möller, A., Peloton, J., Ishida, E. E. O., et al. 2021, *MNRAS*, 501, 3272
- Nordin, J., Brinnet, V., van Santen, J., et al. 2019, *A&A*, 631, A147
- Qin, Y.-J., Zabludoff, A., Arcavi, I., et al. 2024, *MNRAS*
- Qin, Y.-J., Zabludoff, A., Kisley, M., et al. 2022, *ApJS*, 259, 13
- Reyes-Jainaga, I., Förster, F., Muñoz Arancibia, A. M., et al. 2023, *ApJ*, 952, L43
- Ryczanowski, D., Smith, G. P., Bianconi, M., et al. 2020, *MNRAS*, 495, 1666
- Schulze, S., Fransson, C., Kozyreva, A., et al. 2024, *A&A*, 683, A223
- Shappee, B., Prieto, J., Stanek, K. Z., et al. 2014, in *American Astronomical Society Meeting Abstracts*, Vol. 223, American Astronomical Society Meeting Abstracts #223, 236.03
- Taggart, K. & Perley, D. A. 2021, *MNRAS*, 503, 3931
- Tonry, J. L., Denneau, L., Heinze, A. N., et al. 2018, *PASP*, 130, 064505
- Wenger, M., Ochsenbein, F., Egret, D., et al. 2000, *A&AS*, 143, 9
- Williams, R. D., Francis, G. P., Lawrence, A., et al. 2024, *arXiv e-prints*, arXiv:2404.08315
- Yamaoka, H. 2017, in *Handbook of Supernovae*, ed. A. W. Alsabti & P. Murdin, 29
- Zinn, P. C., Grunden, P., & Bomans, D. J. 2011, *A&A*, 536, A103
- Zinn, P. C., Stritzinger, M., Braithwaite, J., et al. 2012, *A&A*, 538, A30

¹¹ <https://cosmostatistics-initiative.org/residence-programs/crp7/>

Appendix A: Nearest neighbor

To compute the distance from the transient to the nearest mask, we assume an origin position at the center of the image from where to calculate the distance. Masked pixels have value 1, whereas background pixels have value 0. To find the nearest masked pixel to the transient, we compare pixel by pixel until a mask is found. First, we check all adjacent pixels (including diagonally adjacent ones) related to the central pixel, starting from left to right and top to bottom. This process is repeated for outer layers until a masked pixel is found or we reach the limits of the 7-pixel threshold. If the distance between the central pixel and the nearest neighbor is not within a 7-pixel radius, we keep that alert in our sample for further checks. The Euclidean distance between the nearest masked pixel and the central pixel is included for the user to assess whether a neighbor is close enough for it to be considered an associated host. The algorithm works as follows:

Data: M : Stamp of the segmented image
 r : Maximum radius for nearest detected source

Result: x_1 : x-axis index of the closest masked source
 x_2 : y-axis index of the closest masked source
 δ : Euclidean distance measured in image pixels
 f : Flag (true for hostless, zero otherwise)

```

 $M_{>0} \leftarrow 1$ 
 $\tau, \delta, f \leftarrow 30, 100, \text{True}$ 
 $x_1, x_2 \leftarrow \text{None}$ 

if  $M_{\tau,\tau} = 1$  then
   $f \leftarrow \text{False}$ 
  return  $\tau, \tau, 0, f$ 
else
  for  $s \in \{1, \dots, r+1\}$  do
     $a \leftarrow \{\tau-1-s, \tau+2+s\}$ 
     $v \leftarrow 0$ 
    for  $i \in a$  do
      if  $(v=0) \vee (v=\tau+1+s)$  then
        for  $j \in a$  do
          if  $M_{i,j} = 1$  then
             $\delta \leftarrow \sqrt{(\tau-i)^2 + (\tau-j)^2}$ 
             $x_1, x_2, f \leftarrow i, j, \text{False}$ 
            return  $x_1, x_2, \delta, f$ 
          end
        else
          for  $j \in \{a_0, a_{|a|}\}$  do
            if  $M_{i,j} = 1$  then
               $\delta \leftarrow \sqrt{(\tau-i)^2 + (\tau-j)^2}$ 
               $x_1, x_2, f \leftarrow i, j, \text{False}$ 
              return  $x_1, x_2, \delta, f$ 
            end
           $v \leftarrow v+1$ 
        end
      end
    end
  end
  return  $x_1, x_2, \delta, f$ 

```

Appendix B: Segmentation masks with SExtractor

A popular image segmentation tool in astronomy is SExtractor¹² (Bertin & Arnouts 1996). This software is largely used for the detection of astronomical sources, background reduction, and photometry of astronomical images, being especially suitable for processing large field-of-view images. However, running SExtractor can be computationally expensive, especially compared to sigma clipping. We decided to compare the performance of both methods considering only those events that have a spectral classification available on the Transient Name Server (TNS)¹³. We find that SExtractor retrieves 149 hostless candidates while sigma clipping retrieves 181 hostless candidates. By visually inspecting each candidate in the search for the presence of a potential host, we find that the SExtractor method has a $\sim 15\%$ contamination while the sigma clipping method has a $\sim 22\%$ contamination. Thus, considering that running SExtractor involves writing and reading files on the disk, which is not ideal when working with large volumes of data; and that the performance of both methods is similar, we favor the simpler sigma clipping as an image segmentation method.

¹² <https://sextractor.readthedocs.io/en/latest/index.html>

¹³ TNS is the International Astronomical Union's official mechanism for reporting new astronomical transients since 2016, <https://www.wis-tns.org/>.

Appendix C: Machine learning classified hostless candidates

Table C.1: Fragment of the hostless candidate list without a reported classification on TNS. The full list can be found as supplementary material.

IAU Name	ZTF Name	R.A. [J2000]	Dec. [J2000]	Class
AT 2016ayj	ZTF19adehksw	03:06:45.60	46:09:12.93	SN*_cand.
AT 2016ayl	ZTF18acwwwsg	05:14:00.67	55:21:57.81	SN*_cand.
AT 2016azn	ZTF22abxlizh	10:06:54.81	-14:25:37.80	AT cand.
AT 2017kn	ZTF18aakpggd	11:54:19.60	57:57:50.77	QSO
AT 2018aod	ZTF23abofayp	03:25:09.82	48:50:19.95	SN cand.
AT 2018cou	ZTF18acxcpmo	14:15:23.73	-20:00:54.17	SN
AT 2018ctv	ZTF18abtgnsi	01:25:52.40	-01:22:01.66	SN
AT 2018cyo	ZTF19aavprpy	22:11:56.27	-04:41:40.50	SN
AT 2018fou	ZTF18abtefbi	23:05:32.51	00:49:02.50	SN
AT 2018his	ZTF22abiflxl	17:49:31.59	17:15:37.23	SN cand.
...